Supplementary Information

Extreme rainfall reduces one-twelfth of China's rice yield

Jin Fu[1]†, Yiwei Jian[1]†, Xuhui Wang[1]†, Feng Zhou[1]*, Laurent Li[2], Philippe Ciais[3,4], Jakob Zscheischler[5], Yin Wang[6], Yanhong Tang[6], Christoph Müller[7], Heidi Webber[8], Bo Yang[9], Yali Wu[10], Qihui Wang[1], Xiaoqing Cui[1], Weichen Huang[1], Yongqiang Liu[11], Shilong Piao[1,12]

†These authors contributed equally to this work.

*Corresponding author. Email: zhouf@pku.edu.cn

This PDF file includes:

Supplementary Table 1 Previous estimates of change in crop yield (ΔY) due to extreme climate events. Data is shown as mean ± standard error, with n representing sample size.

Event*	Crop type	Method	ΔY	n	Reference
Extreme rainfall	Wheat, rice, maize, soy, millet, sorghum	Statistical analysis	−0.6 ± 1.2%	47	1-8
Extreme heat	Wheat, rice, maize, soy	Statistical analysis	−8.1 ± 3.1%	12	9-11
Extreme cold	Rice	Statistical analysis	−10.2 ± 6.5%	10	12
Drought	Wheat, rice, maize, soy,	Statistical analysis	−5.2 ± 2.8%	32	13,14
Event	**Crop type**	**Method**	**Sensitivity of ΔY to rainfall intensity**	**n**	**Reference**
Extreme rainfall	Rice	Statistical analysis	$-0.03 \pm 0.05\%\ (\text{cm h}^{-1})^{-1}$	47	1-3,5-8
Extreme rainfall	Rice	Field observation	$-1.0 \pm 0.2\%\ (\text{cm h}^{-1})^{-1}$	11	15,16

* See definitions in Supplementary Table 2.

Supplementary Table 2 Definition of climate extremes translated from the China meteorological administration

Event	Definitions*	References in Chinese
Extreme heat	A period of abnormally hot weather, if the daily maximum temperature exceeds 35°C.	http://zwgk.cma.gov.cn/zfxxgk/gknr/flfgbz/bz/202107/t20210716_3540198.html
Extreme cold	A period of abnormally cold weather, if daily mean temperature lies below that over the same period in history by one standard deviation.	http://zwgk.cma.gov.cn/zfxxgk/gknr/flfgbz/bz/202102/t20210210_2720477.html
Extreme rainfall	Intense rainfall with short duration, if daily precipitation exceeds 50 mm for rice planting regions in China where mean annual precipitation >400 mm.	http://zwgk.cma.gov.cn/zfxxgk/gknr/flfgbz/bz/202102/t20210210_2720509.html
Drought	A period of unusually low precipitation that produces a shortage of water for plants. It can be defined by different indices, such as standard precipitation index, standardized precipitation evapotranspiration index, and Palmer Drought Severity Index.	http://zwgk.cma.gov.cn/zfxxgk/gknr/flfgbz/bz/202102/t20210210_2719989.html
The other events	It included hail, wind, typhoon and tropical cyclone. A hail storm is a type of storm that is characterized by hail as the dominant part of its precipitation. The size of the hailstones can vary between pea size (6 mm) and softball size (112 mm) and therefore cause considerable damage. Wind is difference in air pressure resulting in the horizontal motion of air. The greater the difference in pressure, the stronger the wind. Wind moves from high pressure toward low pressure. A tropical storm originates over tropical or subtropical waters. It is characterized by a warm-core, non-frontal synoptic-scale cyclone with a low-pressure center, spiral rain bands and strong winds. Depending on their location, tropical cyclones are referred to as hurricanes (Atlantic, Northeast Pacific), typhoons (Northwest Pacific), or cyclones (South Pacific and Indian Ocean).	https://www.docin.com/p-2440560243.html http://zwgk.cma.gov.cn/zfxxgk/gknr/flfgbz/bz/202112/t20211221_4317166.html http://zwgk.cma.gov.cn/zfxxgk/gknr/flfgbz/bz/202102/t20210210_2720508.html

* These definitions are similar with the Emergency Events Database (EM-DAT) at https://www.emdat.be/Glossary.

Supplementary Table 3 Correlations between ΔY and extreme rainfall indices. It included intensity (RX1h, cm h^{-1}), total intensity (RX1hTOT, cm) and its proportion to growing-season total precipitation (R99pPROP, %), frequency in hours (R99f, h), and in proportion to growing season length (R99p, %), event amount (Rg1event, cm $event^{-1}$), and event duration (ERED, hour $event^{-1}$). The thresholds were defined as the 95^{th}, 99^{th}, or 99.9^{th} percentiles of hourly precipitation during growing season in the reference period during 1981–2012 for each site. Extreme rainfall event was defined as events that involve at least one extreme rainfall and for which the break between hourly precipitation lies below 2, 6, 12, and 24 hours. Data is the sensitivity of ΔY to indices (mean ± standard error) estimated from 1,000-time bootstrap analysis. *p<0.05; **p<0.01; ***p<0.001, n.s. for not significant.

Break	Threshold	ΔY v.s. RX1h	ΔY v.s. RX1hTOT	ΔY v.s. R99pPROP	ΔY v.s. Rg1event	ΔY v.s. ERED	ΔY v.s. R99p	ΔY v.s. R99f
2h	95.0^{th}	−2.3 ± 0.6 (***)	−0.3 ± 0.1 (*)	−0.1 ± 0.1 (*)	−0.7 ± 0.1 (***)	−0.3 ± 0.1 (***)	−11.9 ± 5.4 (*)	−0.5 ± 0.2 (*)
	99.0^{th}	−2.2 ± 0.7 (***)	−0.2 ± 0.1 (*)	−0.1 ± 0.1 (n.s.)	−0.6 ± 0.2 (***)	−0.3 ± 0.1 (**)	4.0 ± 17.1 (n.s.)	−0.2 ± 0.7 (n.s.)
	99.9^{th}	−2.6 ± 1.8 (n.s.)	−0.2 ± 0.8 (n.s.)	−0.1 ± 0.6 (n.s.)	−0.7 ± 0.3 (*)	−0.6 ± 0.2 (**)	139.3 ± 152.9 (n.s.)	3.3 ± 5.7 (n.s.)
6h	95.0^{th}	−1.6 ± 0.6 (**)	−0.2 ± 0.1 (*)	−0.1 ± 0.1 (n.s.)	−0.5 ± 0.1 (***)	−0.2 ± 0.1 (***)	−8.5 ± 5.7 (n.s.)	−0.4 ± 0.2 (n.s.)
	99.0^{th}	−1.6 ± 0.7 (*)	−0.2 ± 0.1 (n.s.)	0.0 ± 0.1 (n.s.)	−0.4 ± 0.1 (***)	−0.2 ± 0.0 (***)	−2.1 ± 16.1 (n.s.)	−0.1 ± 0.7 (n.s.)
	99.9^{th}	−2.0 ± 1.7 (n.s.)	−0.1 ± 0.7 (n.s.)	0.2 ± 0.5 (n.s.)	−0.5 ± 0.3 (n.s.)	−0.2 ± 0.2 (n.s.)	−141.27 ± 134.2 (n.s.)	4.0 ± 4.7 (n.s.)
12h	95.0^{th}	−1.7 ± 0.6 (**)	−0.2 ± 0.1 (*)	−0.1 ± 0.1 (n.s.)	−0.5 ± 0.1 (***)	−0.2 ± 0.0 (***)	−10.3 ± 5.5 (n.s.)	−0.5 ± 0.2 (*)
	99.0^{th}	−1.8 ± 0.7 (**)	−0.2 ± 0.1 (n.s.)	0.0 ± 0.1 (n.s.)	−0.3 ± 0.1 (***)	−0.1 ± 0.0 (**)	3.9 ± 15.8 (n.s.)	0.1 ± 0.7 (n.s.)
	99.9^{th}	−2.1 ± 1.8 (n.s.)	−0.1 ± 0.7 (n.s.)	0.0 ± 0.5 (n.s.)	−0.7 ± 0.4 (n.s.)	−0.3 ± 0.2 (n.s.)	146.73 ± 137.2 (n.s.)	3.5 ± 5.0 (n.s.)
24h	95.0^{th}	−1.4 ± 0.6 (*)	−0.2 ± 0.1 (*)	−0.1 ± 0.1 (*)	−0.4 ± 0.1 (***)	−0.2 ± 0.0 (***)	−12.5 ± 5.1 (*)	−0.6 ± 0.2 (**)
	99.0^{th}	−1.9 ± 0.7 (**)	−0.3 ± 0.1(*)	−0.1 ± 0.1 (n.s.)	−0.3 ± 0.1 (***)	−0.1 ± 0.0 (**)	−17.7 ± 15.9 (n.s.)	−0.8 ± 0.7(n.s.)
	99.9^{th}	−2.6 ± 1.8 (n.s.)	−0.1 ± 0.8 (n.s.)	0.3 ± 0.5 (n.s.)	−0.4 ± 0.3 (n.s.)	−0.2 ± 0.1 (n.s.)	144.9 ± 145.6 (n.s.)	4.2 ± 5.0 (n.s.)

Supplementary Table 4 Model equations derived from the best-fit structural equation model

Equation	Description*
Change in effective panicle per unit land area (ΔEP)	
$\Delta EP = a_1 \cdot \Delta N_{ut} + b_1$	ΔEP: relative change in effective panicle during vegetative phase (%), ΔN_{ut}: relative change in N uptake per tiller of rice during vegetative phase (%), $a_1 = 0.262$, $b_1 = -1.644$.
$\Delta N_{ut} = a_2 \cdot \Delta N_{loss} + b_2$	ΔN_{ut}: relative change in N uptake per tiller during vegetative phase (%), ΔN_{loss}: change in N loss during vegetative phase induced by extreme rainfall (kg N ha^{-1}), $a_2 = -1.026$ and $b_2 = 7.054$.
$\Delta N_{loss} = (N_{l1} + N_{r1}) - (N_{l0} + N_{r0})$ for model performance assessment	ΔN_{loss}: soil N loss (kg N ha^{-1}), N_l: change in N loss via leaching (kg N ha^{-1}), N_r: change in N loss via runoff (kg N ha^{-1}), with the subscript 1 for extreme rainfall treatment and 0 for control.
$N_l = \left(0.0463 + 0.0037 \cdot \frac{P}{C \cdot L}\right) \cdot (F + \gamma \cdot D - U)$ for historical simulations and future projections	P: precipitation during the vegetative phase (mm), C: clay content (%), L: layer thickness or rooting depth (m), F: mineral and manure fertilizer N (kg N ha^{-1} yr^{-1}), γ: the decomposition rate of manure matter (% yr^{-1}), D: soil N density (kg N ha^{-1}), U: N uptake by crop (kg N ha^{-1}), according to ref.[17].
$N_r = EFP \cdot C_r + H_w \cdot (C_p - C_r) \cdot (1 - e^{-\frac{EFP}{H_r}}) + 2.2 \cdot C_p \cdot W \cdot T$ for historical simulations and future projections	EFP: effective precipitation per event during the vegetative phase, defined as the difference between precipitation and the sum of canopy interception and subsurface water fluxes (mm event^{-1}), C_r: mean N concentration of rainfall (mg L^{-1}), C_p: mean N concentration of ponded water (mg L^{-1}), H_w: mean ponded water level (mm), H_r: weir outlet height (mm), W: soil-water exchange velocity (cm s^{-1}), T: rainfall duration (s), according to ref.[18].
Change in filled grains per panicle (ΔFG)	
$\Delta FG = c \cdot KE_{re} + d \cdot KE_{ri} + e \cdot \Delta N_{up} + f$	ΔFG: relative change in filled grain, KE_{re}: time-specific kinetic energy during reproductive phase (J m^{-2} h^{-1}), KE_{ri}: time-specific kinetic energy during ripening phase (J m^{-2} h^{-1}), ΔN_{up}: relative change in N uptake per panicle due to the change in ΔN_{ut}, $c = -0.00424$, $d = -0.00115$, $e = 0.139$, $f = -3.676$.
$\Delta N_{up} = a_3 \cdot \Delta N_{ut} + b_3$	This correlation is confirmed by previous work[19], $a_3 = 0.723$, $b_3 = 1.592$.
$KE = 1288.17 \cdot \mu^{-1.34} \cdot Int^{(1+1.34 \cdot \beta)}$	Int: actual rainfall intensity ($mm\ h^{-1}$), following Salles et al.[20]. Constants that are linked to the type of microphysical process dominant in the raindrop growth. Since stratiform rain dominates in summer East Asia[21], we use constants corresponding to stratiform rain ($\mu = 40$ and $\beta = 0.21$) in this study.
$Int = \begin{cases} 0.736 \cdot D^{4.525}, & for\ D < 2.531mm \\ 10^{1.019 \cdot D - 0.891}, & for\ D \geq 2.531\ mm \end{cases}$	D: diameter of raindrop (mm), its correlation with Int is according to Nanko et al.[22].

Supplementary Table 5 Physicochemical properties of topsoil in the experimental site

Soil depth	0-20 cm	20-40 cm	40-60 cm	60-80 cm	80-100 cm
SOM	20.4	11.6	7.4	6.4	6.3
STN	1.2	0.8	0.6	0.5	0.6
STP	0.8	0.8	0.7	0.8	0.7
NH_4-N	2.4	1.9	1.7	1.8	1.5
NO_3-N	8.6	8.2	6.6	5.4	4.1
Olsen-P	29.4	22.2	14.4	31.8	15.0
Sand	0.4	0.6	0.4	0.7	0.2
Silt	79.8	82.2	81.8	80.3	76.5
Clay	19.8	17.2	17.8	19	23.3

The table depicts soil organic matter (SOM), soil total nitrogen (STN) and soil total phosphorus (STP) in g kg^{-1}, soil ammonium nitrogen (NH_4-N), soil nitrate nitrogen (NO_3-N), and soil available phosphorus (Olsen-P) in mg kg^{-1}, as well as soil texture including sand, silt and clay content in %.

Supplementary Table 6 Model input data for historical simulations and future projections

Input data	Temporal resolution	Spatial resolution	Data source	Ref.
Historical simulations				
Climate forcing*	Daily	0.5°	CRU-NECP v8	23
Atmospheric CO_2 concentration	Annual	--	Ed Dlugokencky and Pieter Tans, NOAA/GML	24
Extreme rainfall intensity and event amount	Half hourly	0.1°	GPM (IMERG), version 6.0	25
Transplanting date	Fixed value	0.1° (interpolated from site-level observations)	National agrometeorological observation network	26
N loss via runoff	Event-based	0.1°	Calculated based on Table S4	18
N loss via leaching	Seasonal	0.1°	Calculated based on Table S4	17
N application rate	Seasonal	1km		27
Rice sowing area	Fixed value	1km		27
Future projections				
Climate forcing*	Daily	0.5°	IPSL earth system model	28
Atmospheric CO_2 concentration (RCP4.5, RCP8.5)	Annual	--		29
Extreme rainfall intensity and event amount	Half hourly	0.5°	IPSL earth system model	28
Transplanting date	Fixed value	0.1° (interpolated from site-level observations)	National agrometeorological observation network (consistent with historical simulation)	26
N loss via runoff	Event-based	0.1°	Calculated based on Table S4	18
N loss via leaching	Seasonal	0.1°	Calculated based on Table S4	17
N application rate	Seasonal	1km	Same as historical simulations	27
Rice sowing area	Fixed value	1km	Same as historical simulations	27

* It includes daily maximum temperature, daily minimum temperature, precipitation rate, surface wind, near-surface air temperature, surface air pressure, air specific humidity, surface downwelling, shortwave radiation, surface downwelling, and longwave radiation.

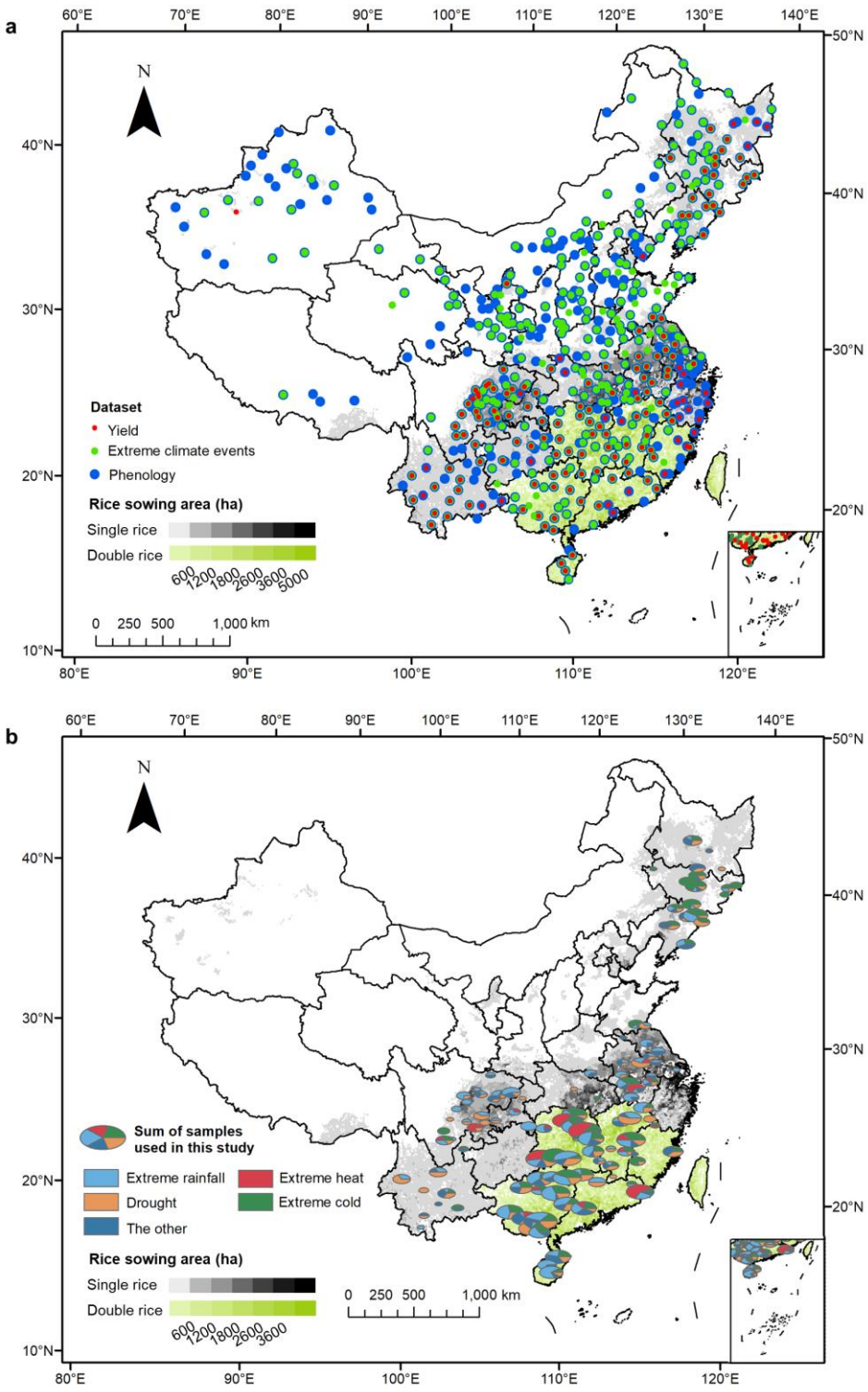

Supplementary Fig. 1 Field observation network of rice yield, phenology, and extreme climate events during 1999-2012. Note that panel **b** shows the distribution of the 707 control-treatment pairs filtered by a window searching strategy.

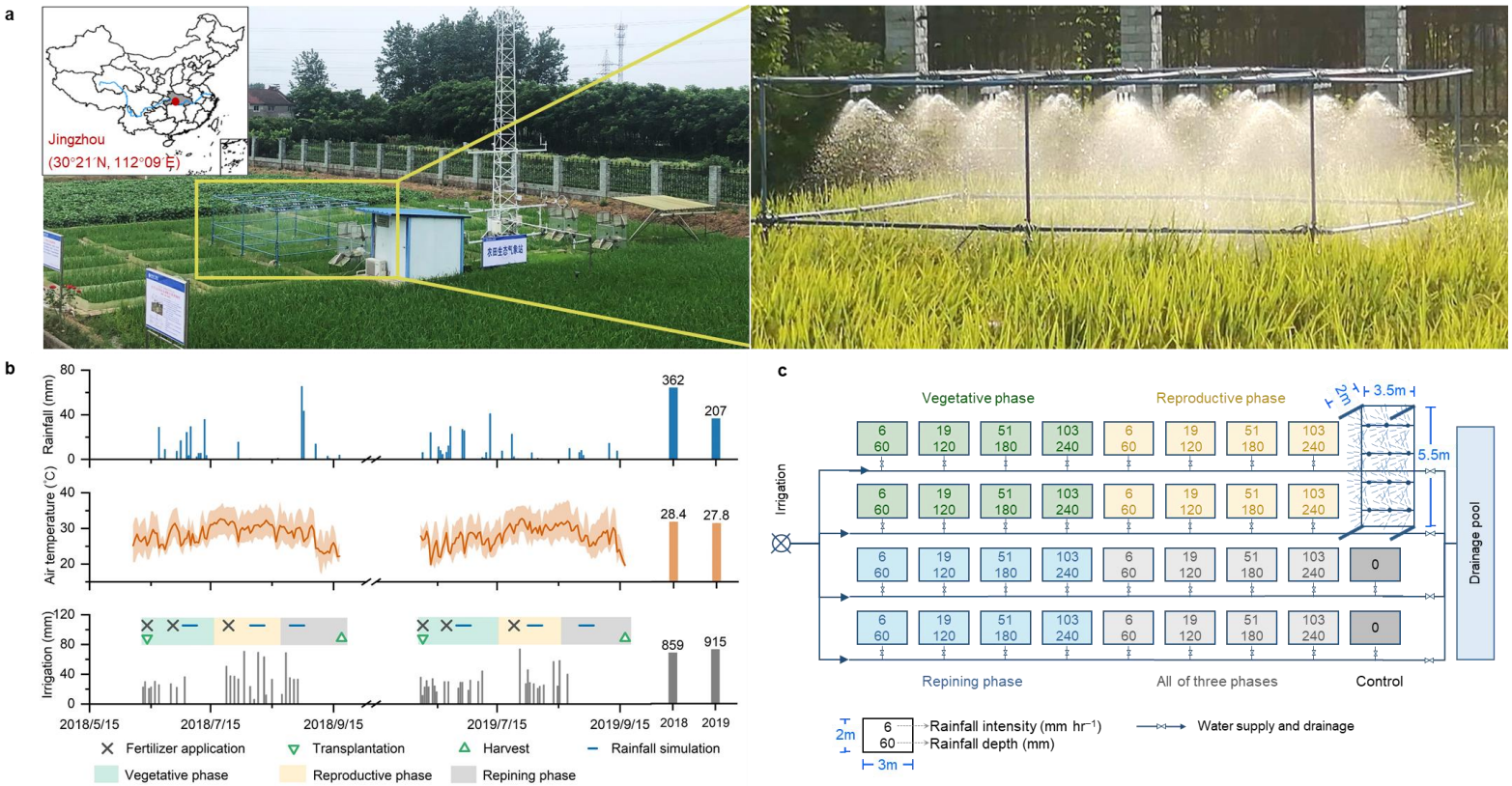

Supplementary Fig. 2 Field setup of the main experiment conducted from 2018 to 2019. a. Field location and the artificial rainfall simulation system. **b**. Climate, fertilization, and irrigation conditions. **c**. Schematic diagram of field layouts and rainfall manipulations. Rainfall manipulations were conducted in 3rd July - 6th July in vegetative phase, 6th August - 9th August in reproductive phase, and 26th August - 29th August in repining phase of 2018, and in 27th June - 30th June in vegetative phase, 2nd August - 5th August in reproductive phase, and 28th August -31st August in repining phase of 2019. Filled colors of panel **c** corresponds to the manipulations conducted in different growth phases.

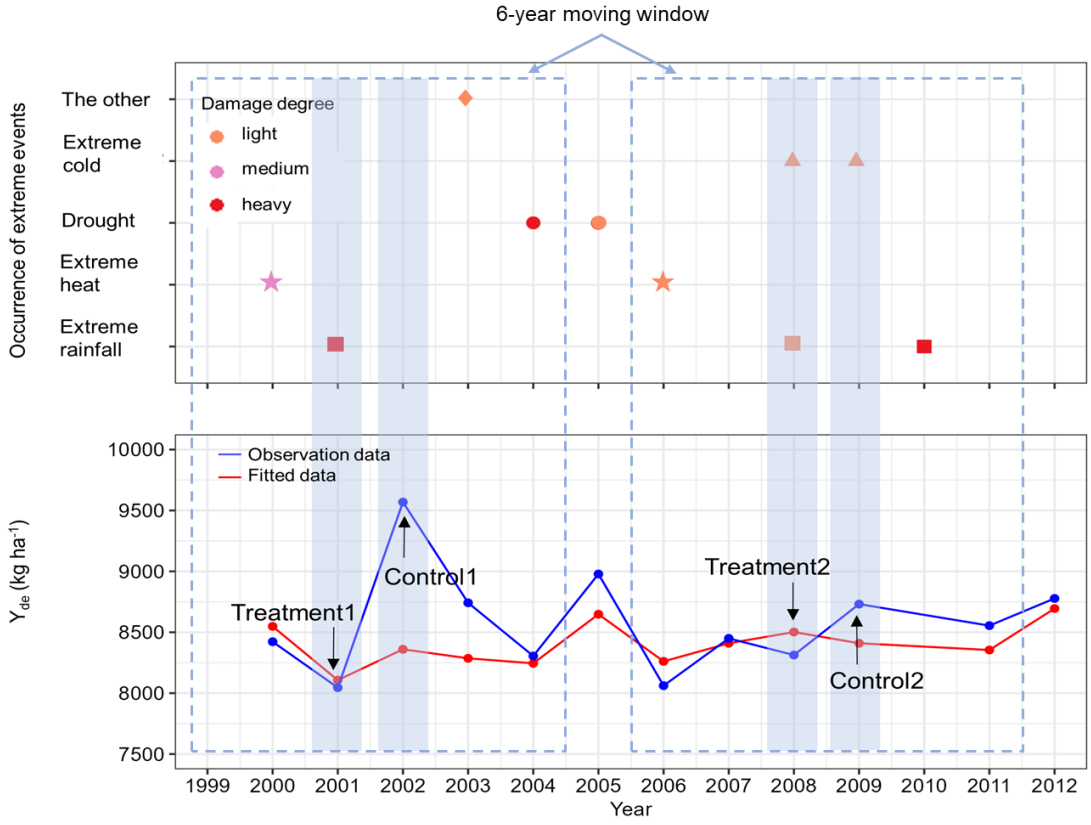

Supplementary Fig. 3 An example to identify the control-treatment pairs using a window searching strategy. Points in the top panel represent for extreme events for which colors indicate their damage degree. Blue dot-line in the bottom panel represents for annual actual rice yields, while red for fitted yields. Blue dotted boxes show the 6-year moving windows, within which all available control-treatment pairs can be identified, being shown as blue shadows.

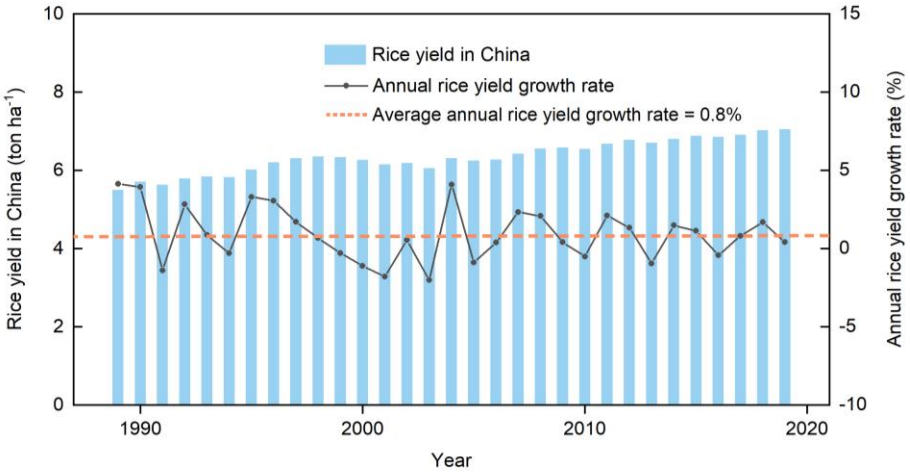

Supplementary Fig. 4 Annual rice yield growth from 1969 to 2019 in China. Data was obtained from the FAOSTAT[30]. The dotted orange line indicates for the average annual growth (0.8%).

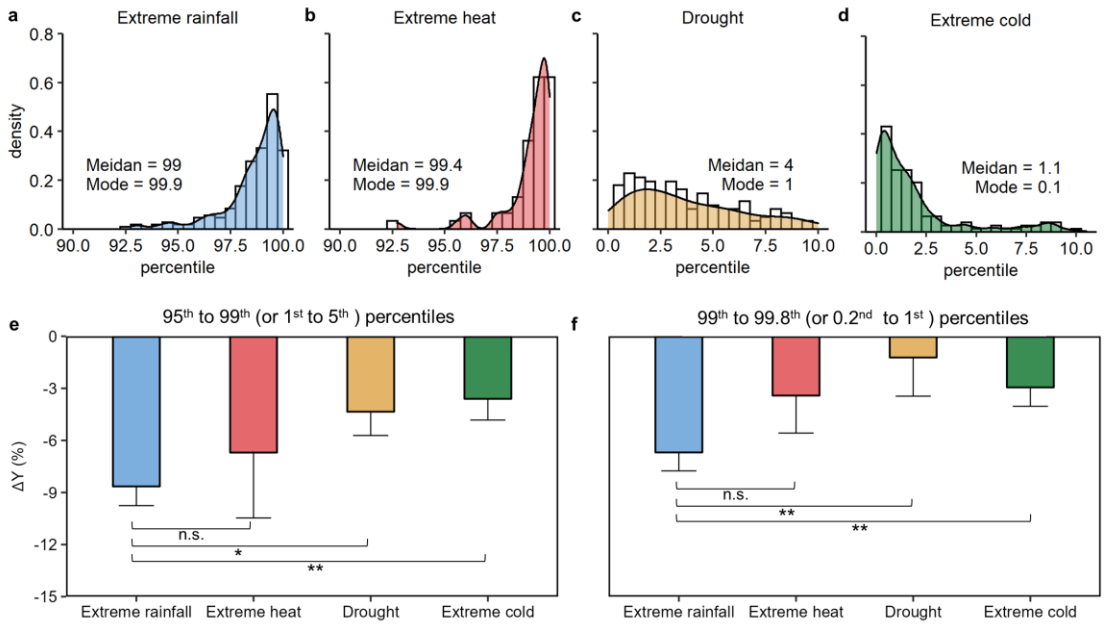

Supplementary Fig. 5 Comparison in the effects of different extreme events with similar percentiles. a. Histogram with kernel density estimation (hereinafter referred to as histogram) of extreme rainfall based on data of the maximum hourly precipitation recorded in given days for different sites and treatment years, **b**. Histogram of extreme heat based on data of maximum hourly air temperature recorded in given days for different sites and treatment years, **c**. Histogram of drought based on data of the minimum standardized precipitation evapotranspiration index[31] recorded in given days for different sites and treatment years, **d**. Histogram of extreme cold based on data of the minimum hourly air temperature recorded in given days for different sites and treatment years, **e**. Comparison of effects of extreme events with the similar percentiles from 95th to 99th for extreme heat and rainfall and from 1st to 5th for extreme cold and drought, **f**. Comparison of effects of extreme events with the similar percentiles from 99th to 99.8th for extreme heat and rainfall and from 0.2nd to 1st for extreme cold and drought. For each of the 707 control-treatment pairs, we calculated the percentile of climate extremes recorded in given days for each site in reference to the base period 1981–2012. The data used was from the site observations run by the China Meteorological Administration (CMA). Both median and mode values were estimated.

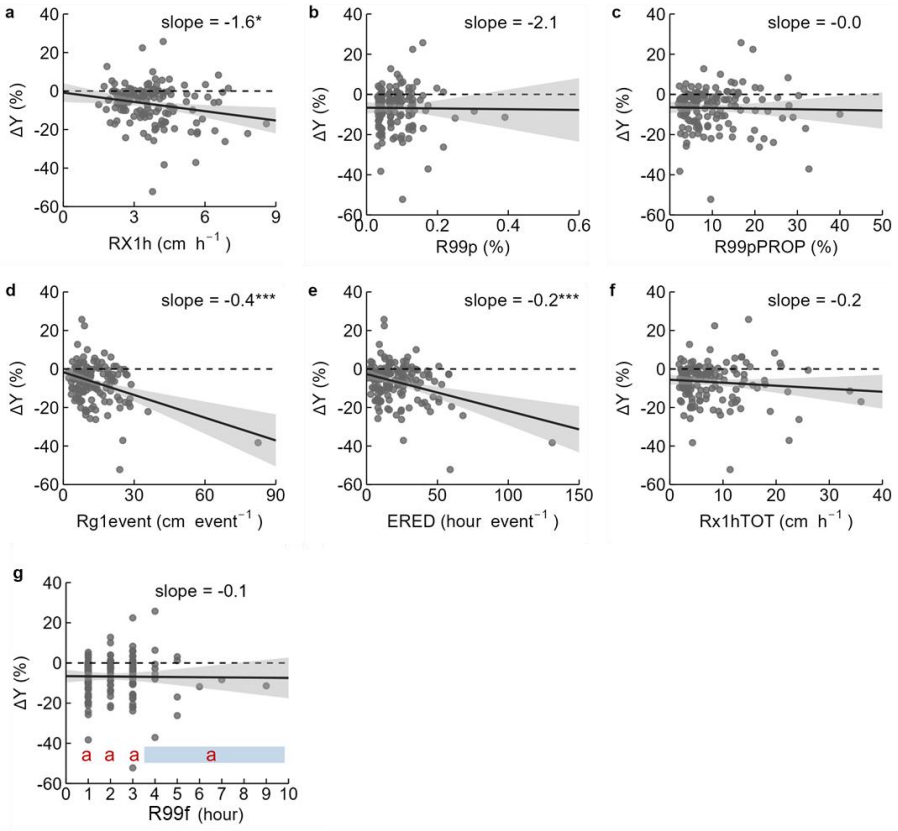

Supplementary Fig. 6 Correlations between ΔY and extreme rainfall. a. Intensity as the maximum hourly precipitation when exceeding the threshold (RX1h), for which we identified the 99th percentile of hourly precipitation during growing season in the reference period 1981–2012 as the site-specific threshold. **b**. Frequency as the fraction of the hours when hourly precipitation exceeds the threshold to the length of rice growing season in hours (R99p). **c**. Proportion as the sum of hourly precipitation that exceeds the threshold divided by the growing-season total precipitation (R99pPROP). **d**. Event amount as the precipitation amount averaged for extreme rainfall events that involve at least one extreme rainfall and for which the break between hourly precipitation does not exceed 6 hours (Rg1event). **e**. Event duration as the total hours of extreme rainfall events during rice growing season divided by event numbers (ERED). **f**. Total intensity as the sum of hourly precipitation when exceeding the threshold (RX1hTOT, cm h^{-1}). **g**. Frequency as hours when hourly precipitation exceeds the threshold to the length of rice growing season in hours (R99f, hours). Threshold of extreme hourly rainfall was defined as the 99th percentile. Rainfall event was defined with the break between rainfall no more than 6 hours. Lines are the slope values and shaded areas refer to the 95% confidence interval estimated from 1,000-time bootstrap analysis. *p<0.05; **p<0.01; ***p<0.001. The Kruskal-Wallis Rank Sum Test and Dunn's test were used for testing significance among R99f, since its neither conform to a normal distribution (Shapiro-Wilk test, p<0.001) nor meet the homogeneity of variances (Bartlett's test, p=0.001). Blue shadows in panel **g**. covered frequency≥4, with the same letters indicating for not significant differences in comparison with other frequencies, α=0.05.

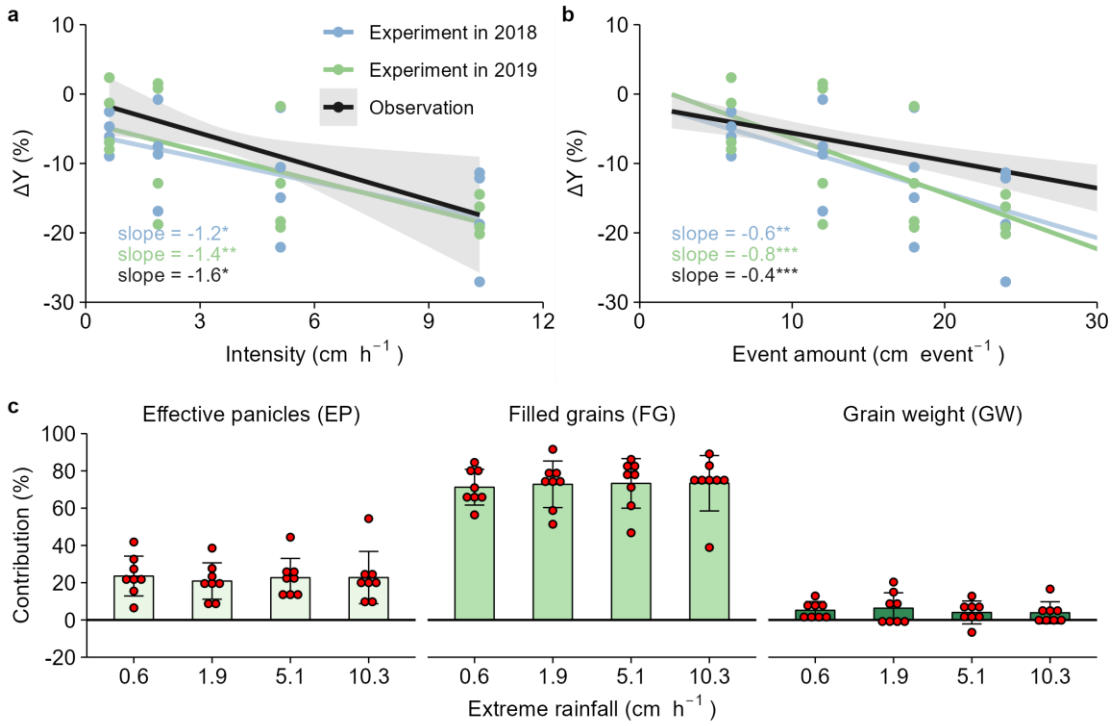

Supplementary Fig. 7 Experimental evidence of the extreme rainfall-rice yield relationship. a. ΔY v.s. extreme rainfall intensity. **b**. ΔY v.s. extreme rainfall event amount; for panels **a** and **b**, no significant differences were found between the slope values from national observations and rainfall manipulative experiments, or between two experiment years. **c**. Attribution of relative changes in effective panicle per unit land area (ΔEP), filled grains per panicle (ΔFG), and grain weight (ΔGW) to ΔY, following the Kaya identity approach[32], that is ΔY = ΔEP + ΔFG + ΔGW.

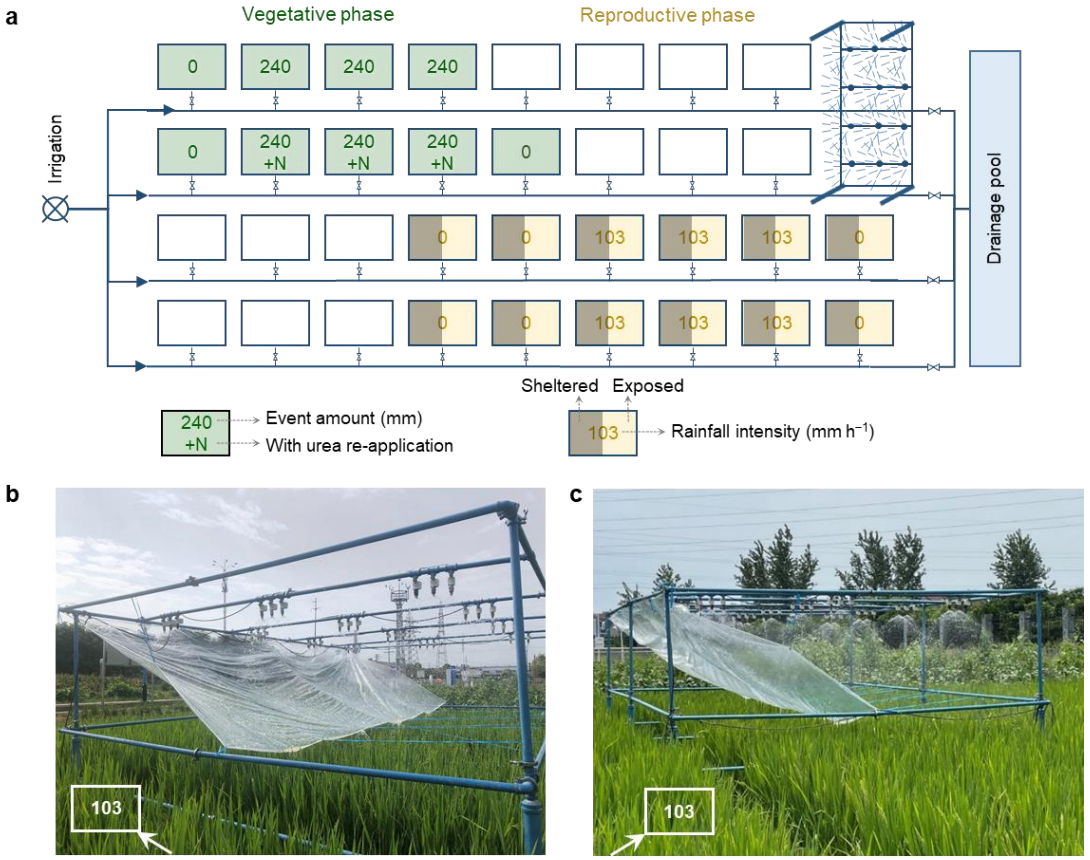

Supplementary Fig. 8 Field setup of the supplementary experiment conducted in 2021. a. Field layout of two supplementary experiments. **b** to **c**. Artificial rainfall simulation system with transparent rain shelter during reproductive phase, with the views from the right and left corners, respectively.

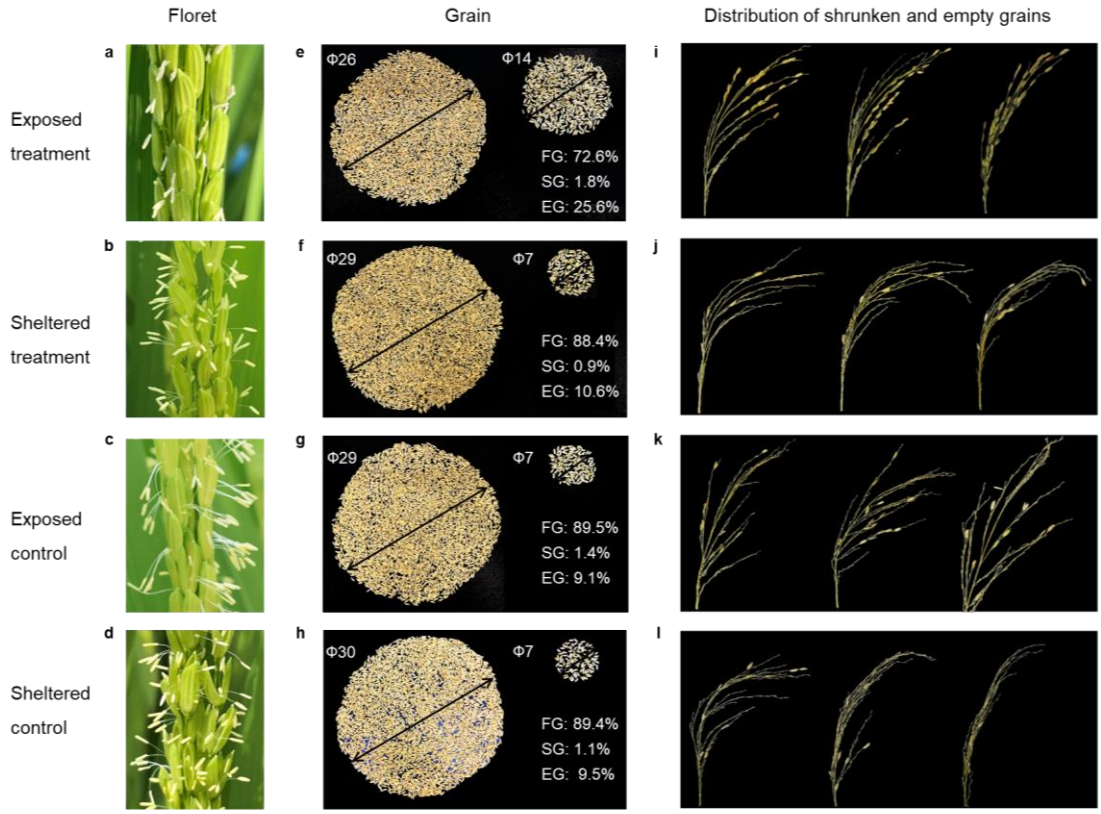

Supplementary Fig. 9 Differences in floret, grains, and grain distribution revealed by the first supplementary experiment. Panels **a** to **d** indicate that florets adhered to the surface of spikelet due to rainfall, while keeping normal for sheltered treatments and the controls. Panels **e** to **h** indicate that rainfall induced less filled grains (FG) but more empty or shrunken grains (EG or SG) than the sheltered treatments and the controls, based on 6 panicles randomly selected. Panels **i** to **l** indicate that empty or shrunken grains were found mainly in the upper part of the panicles for the exposed treatments, while in general distributing evenly along the panicles for the sheltered treatments and the controls, based on 3 typical panicles.

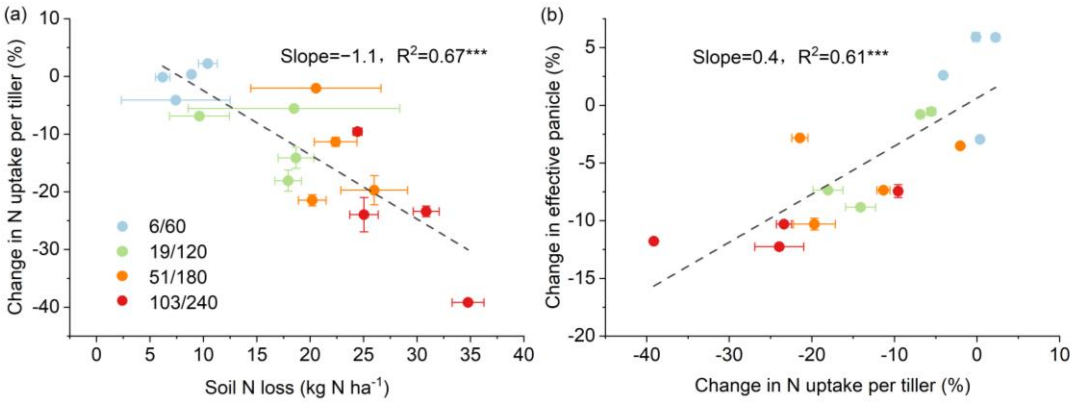

Supplementary Fig. 10 Experimental relationships between soil N loss and changes in effective panicle. a. Soil N loss v.s. Change in N uptake per tiller, **b**. Change in N uptake per tiller v.s. Change in effective panicle. In the legend, numbers before the slash indicate for extreme rainfall intensity (mm h^{-1}), and numbers after indicate for event amount (mm).

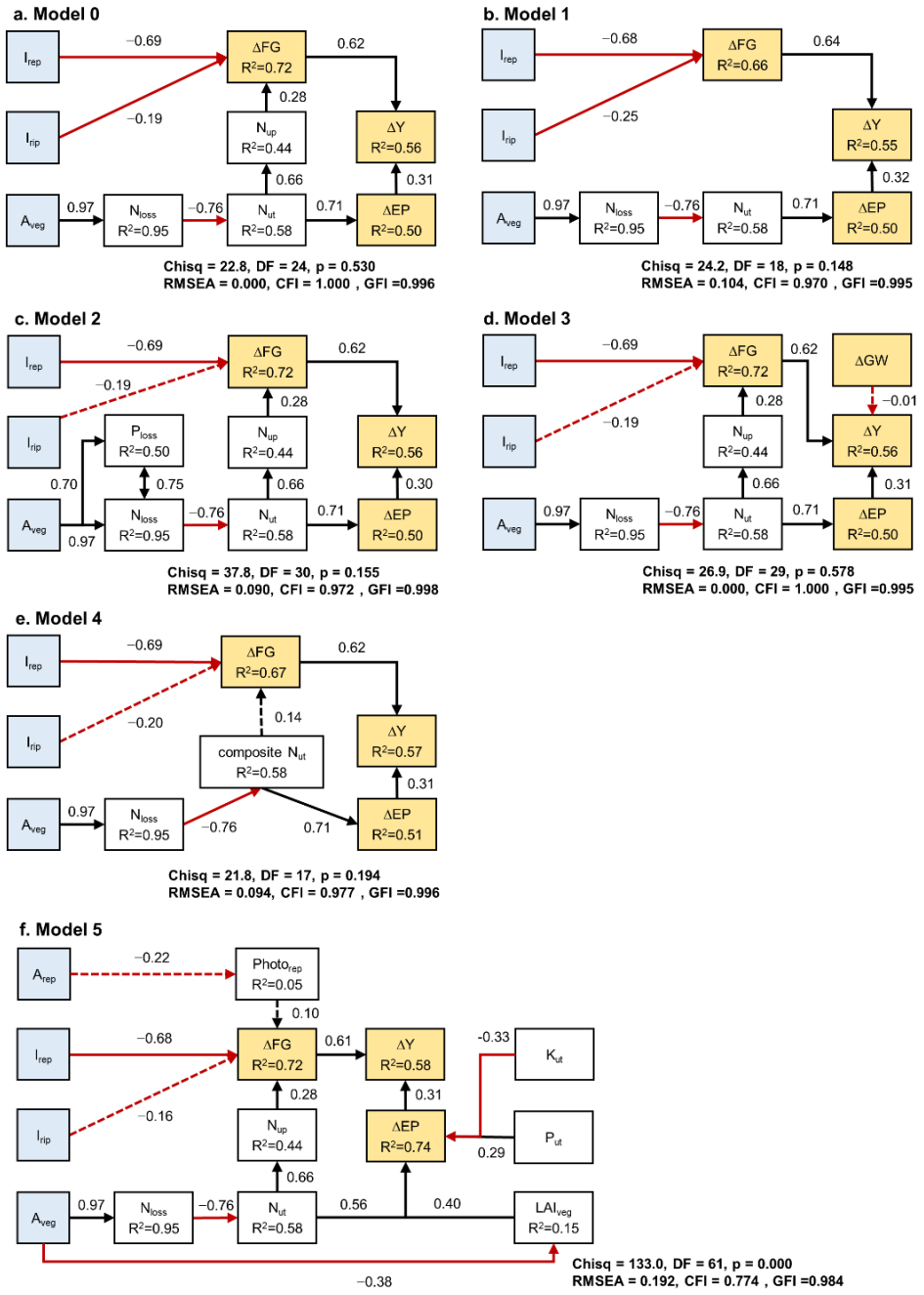

Supplementary Fig. 11 Structural equation modeling for hypothesis tests. A_{veg}, extreme rainfall event amount in vegetative phase; I_{rep} and I_{rip}, extreme rainfall intensity in reproductive and ripening phases, respectively; ΔY, ΔEP, and ΔFG, relative changes in rice yield, effective panicle, and filled grains, respectively; N_{loss}, N_{ut}, and N_{up}, relative changes in soil N loss, per-tiller N uptake during vegetative phase and per-panicle N uptake during reproductive phase, respectively; P_{loss}, P_{ut}, K_{ut}, relative changes in soil P loss, per-tiller P uptake, and per-tiller K uptake during vegetative phase, respectively; $Photo_{rep}$, photosynthetic rate in reproductive phase; LAI_{veg}, leaf area index in vegetative phase. Solid black (red) arrows (with standardized path coefficients) indicate significant positive (negative) effects ($p<0.05$), while dotted lines for insignificant effects.

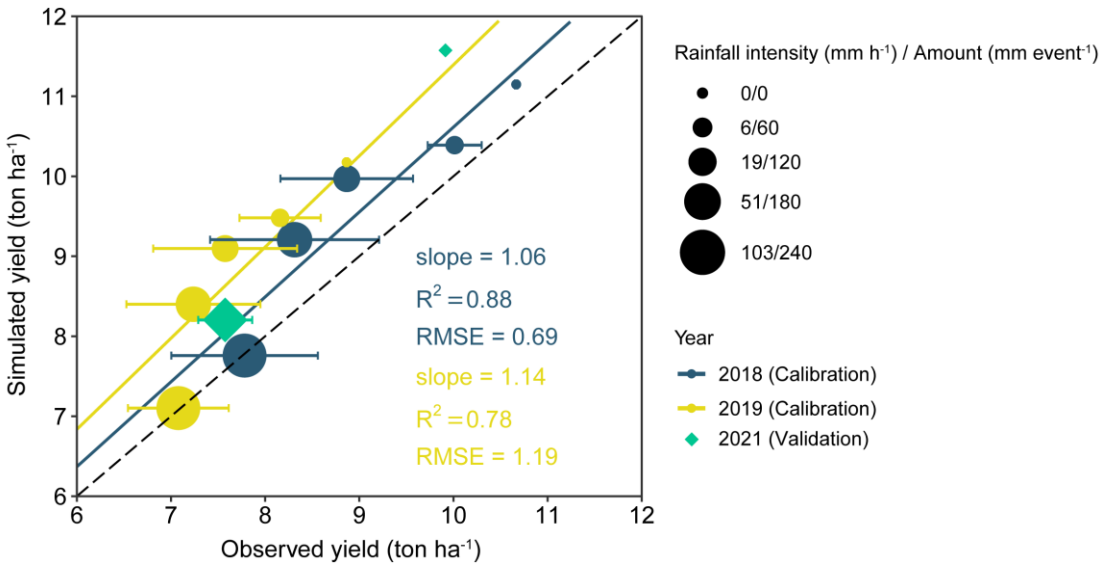

Supplementary Fig. 12 Performance of the improved ORCHIDEE-Crop model for simulating rice yields. Observed yield is obtained from the main experiment in 2018, 2019 and the supplementary experiment in 2021, showing as mean ± standard deviation. Dot size refers to rainfall levels, while colors for three experiment years. Parameters include slope, the coefficient of determination (R^2) and mean root mean square error (RMSE).

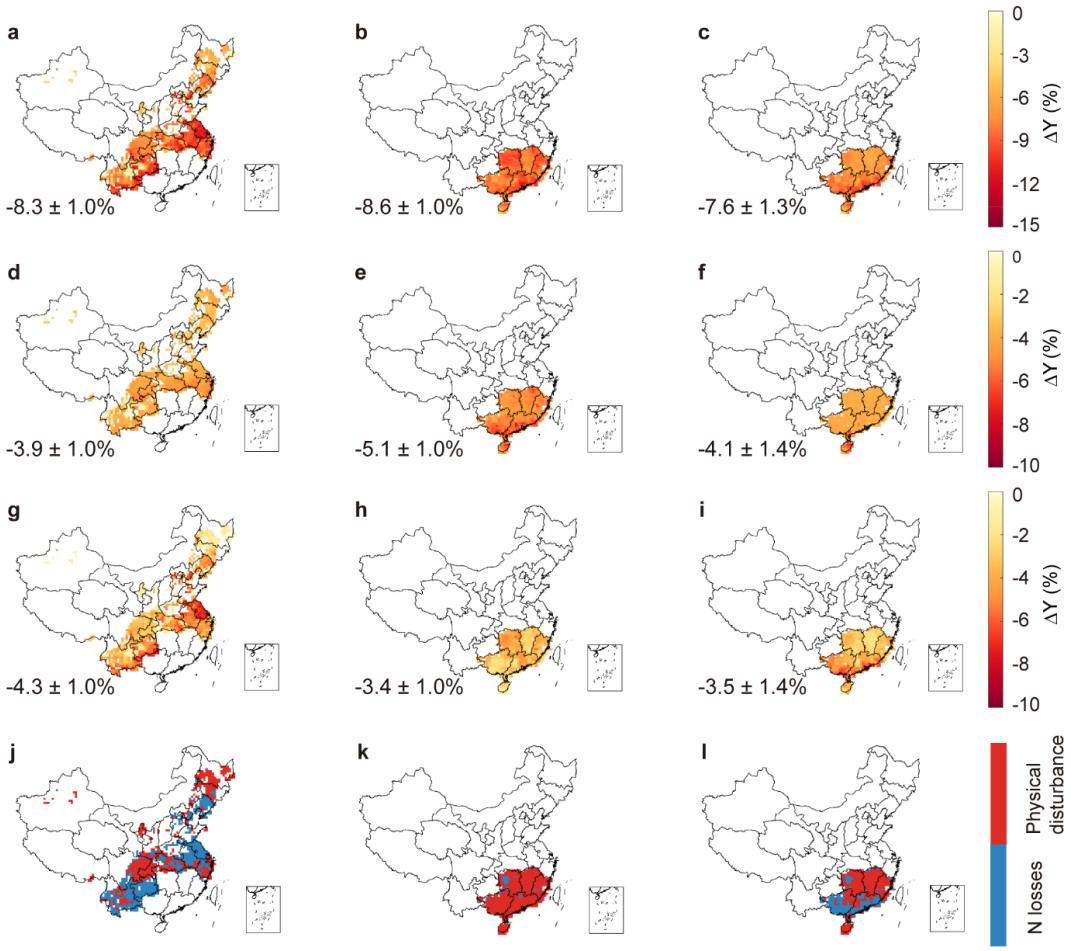

Supplementary Fig. 13 Regional assessments of rainfall-induced rice yield reductions in 2001-2016 based on the improved model. a-c. Effects of rainfall-induced physical disturbance and N losses; **d-f.** Effects of rainfall-induced physical disturbance; **g-i.** Effects of rainfall-induced N losses. **j-l.** Dominant pathways of extreme rainfall impacts on rice yield. Left column is for single rice, middle column is for early rice, and right column is for late rice. The number in each panel indicates national mean relative change in rice yield weighted by sowing area and its standard error for interannual variability.

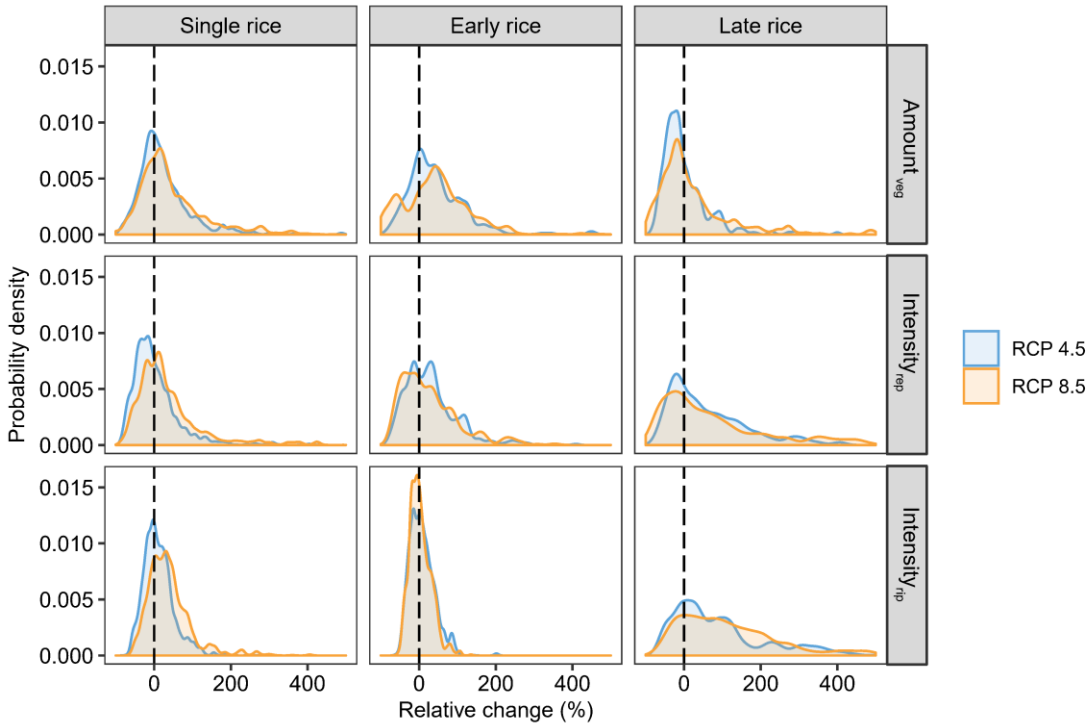

Supplementary Fig. 14 Relative change in extreme rainfall in 2085-2100 compared to that in 2001-2016 under RCP 4.5 and RCP 8.5. The relative change is calculated as the difference between IPSL-projected and IPSL-simulated extreme rainfall indices, including extreme rainfall event amount in vegetative phase ($Amount_{veg}$), extreme rainfall intensities in reproductive phase ($Intensity_{rep}$) and in ripening phase ($Intensity_{rip}$).

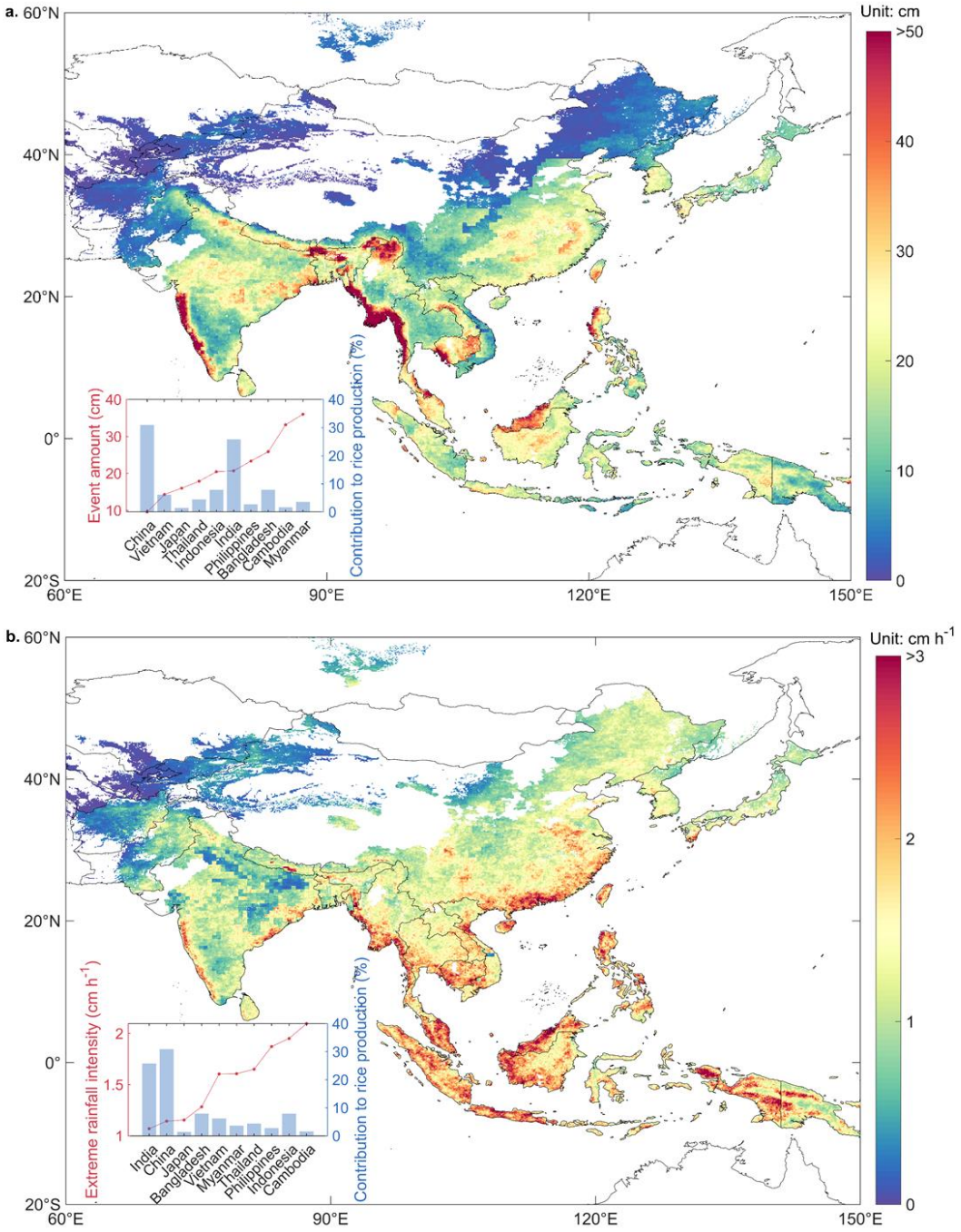

Supplementary Fig. 15 Patterns of extreme rainfall across the Asian rice fields. a. Cumulative extreme rainfall event amounts during vegetative phase averaged over the period 2001-2016, **b.** Extreme rainfall intensity during reproductive phase averaged over the period 2001-2016. The definitions of extreme rainfall and its event can be found in the Methods. Data sources of hourly precipitation, rice phenology, rice production are the GPM IMERGv6[25], Jägermeyr et al.[33], and the FAOSTAT[30], respectively.

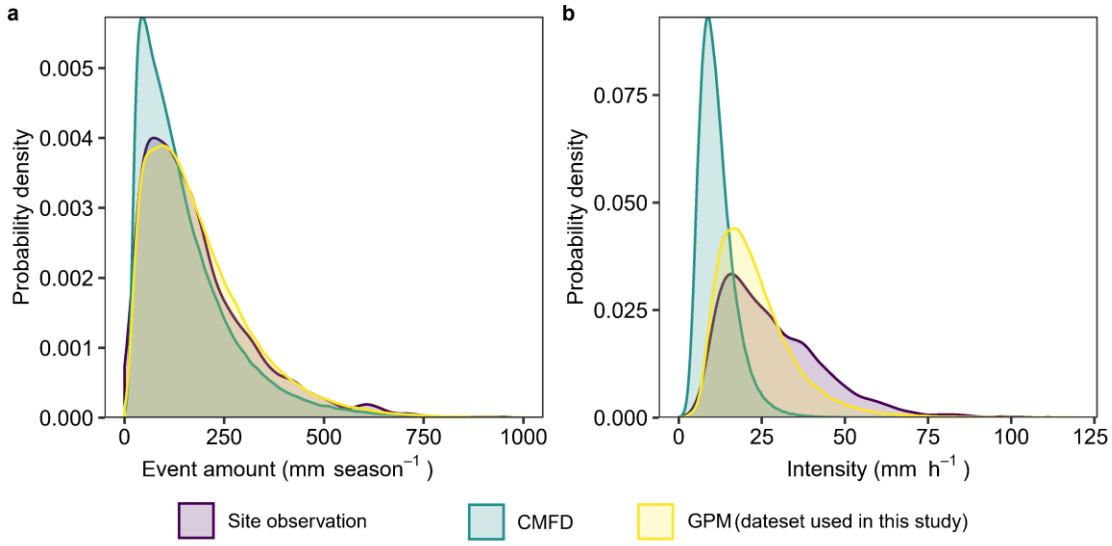

Supplementary Fig. 16 Probability distributions of extreme rainfall from three data sets during 2001-2016. a. the Extreme rainfall event amount during rice growing season; **b.** Extreme rainfall intensity during rice growing season. Three data sets include the site observation from the China Meteorological Administration (CMA), the China Meteorological Forcing Dataset (CMFD, http://data.tpdc.ac.cn/en/data/8028b944-daaa-4511-8769-965612652c49/), and global precipitation measurement (GPM) IMERGv6, ref[25].

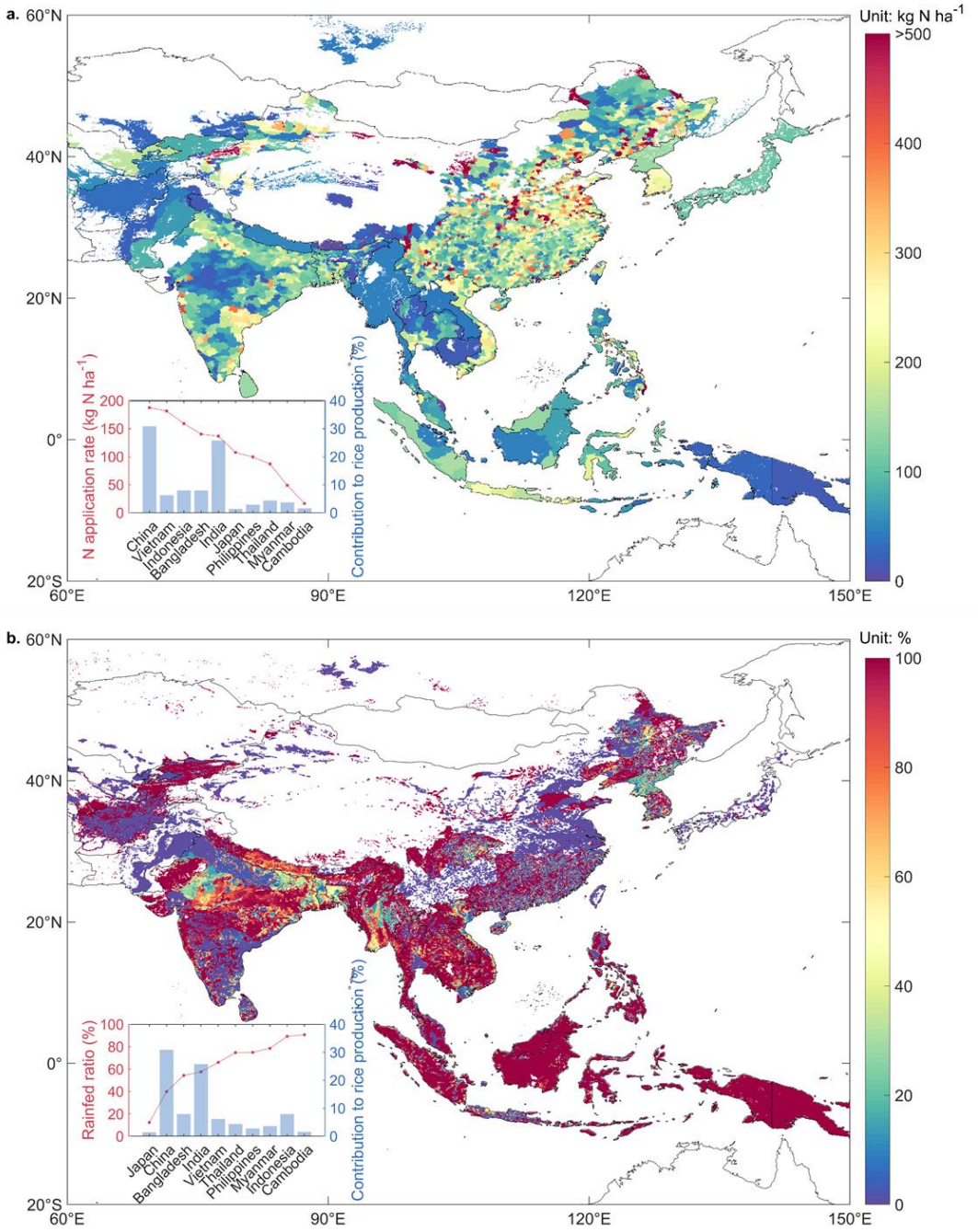

Supplementary Fig. 17 N application rates and rainfed ratios across the Asian rice fields. a. N application rate[27], **b**. rainfed ratio[30].

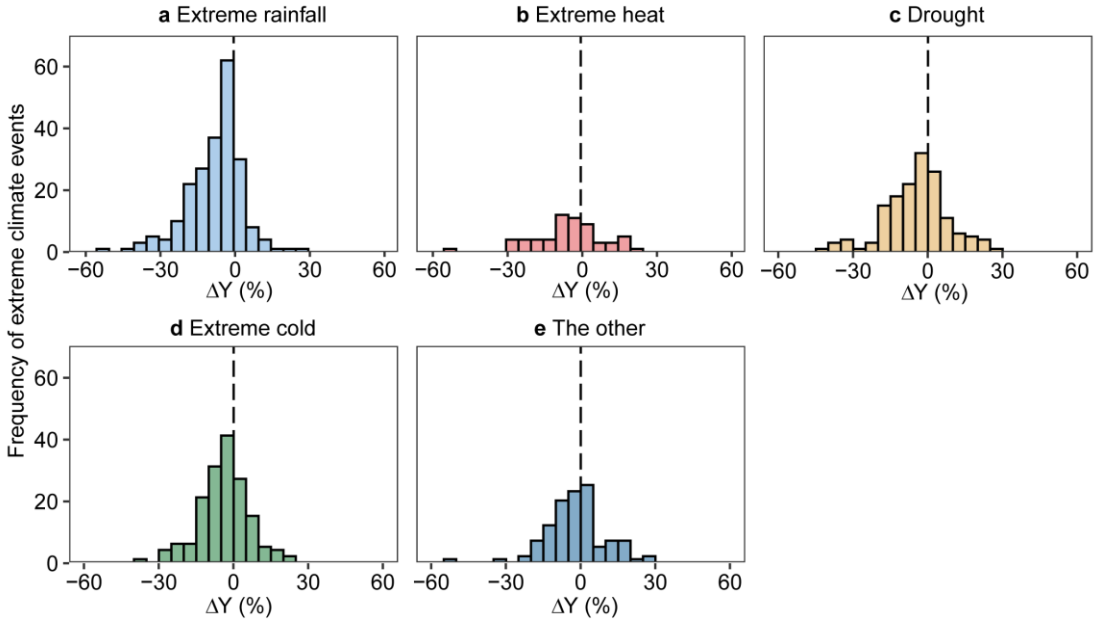

Supplementary Fig. 18 Frequency of individual yield responses to climate extremes. a. ΔY due to extreme rainfall, **b**. ΔY due to extreme heat, **c**. ΔY due to drought, **d**. ΔY due to extreme cold, **e**. ΔY due to the other events (typhoon and tropical cyclones). A preponderance of moderately negative values (falling towards the left areas of the dashed lines) underlies the negative mean climate extreme response signals, with a limited influence of a few outliers (those at the right areas of the dashed lines).

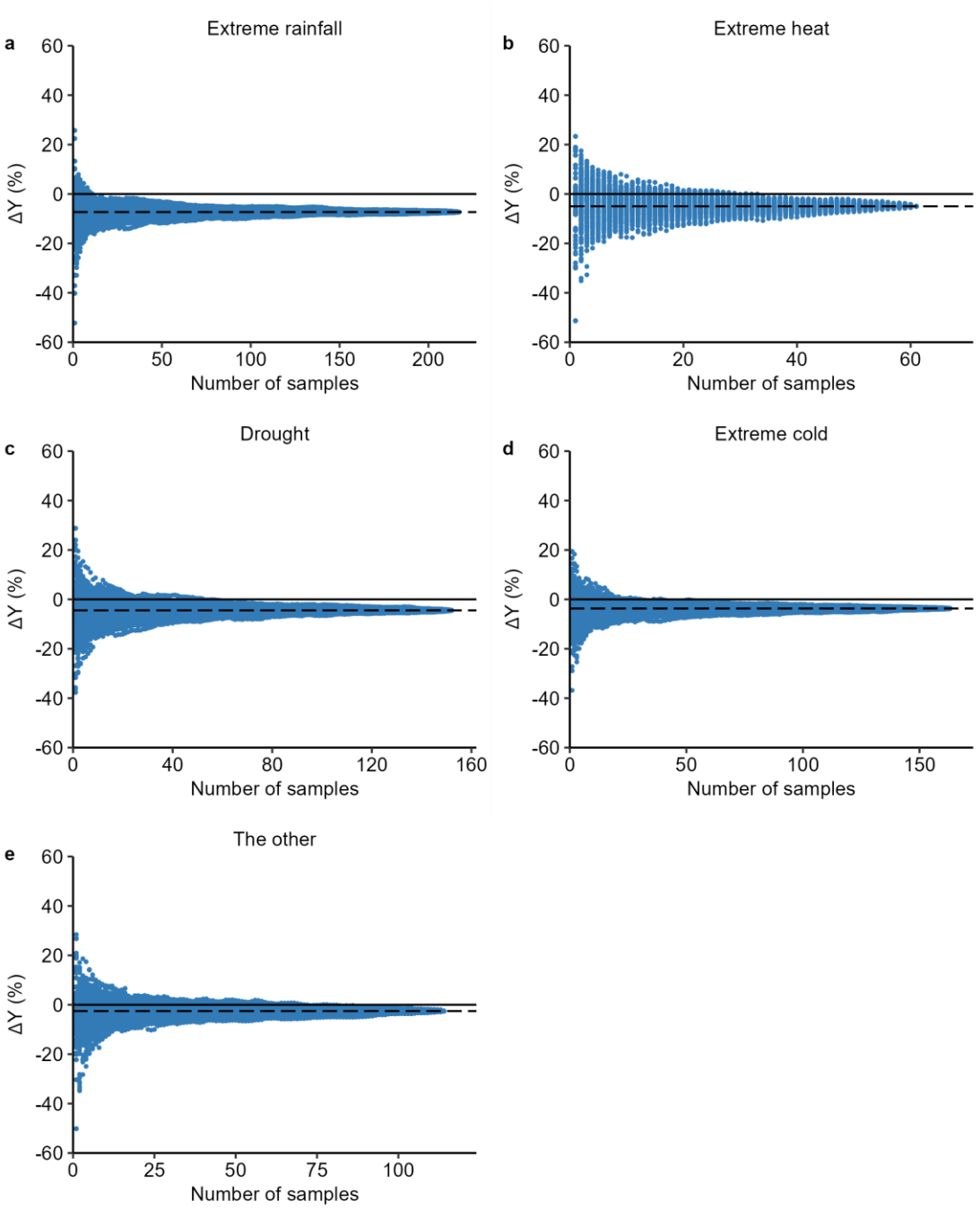

Supplementary Fig. 19 Influence of sample size on ΔY. a. ΔY due to extreme rainfall, **b**. ΔY due to extreme heat, **c**. ΔY due to drought, **d**. ΔY due to extreme cold, **e**. ΔY due to the other events (typhoon and tropical cyclones). Estimated mean yield deficit for extreme climate events in 200 sub-samples with size of (1, 2, …, n) (points). Dotted grey line shows the final estimated mean yield deficit. Most of the initial variability at low sample sizes dissipates into the mean at well below the actual sample size.

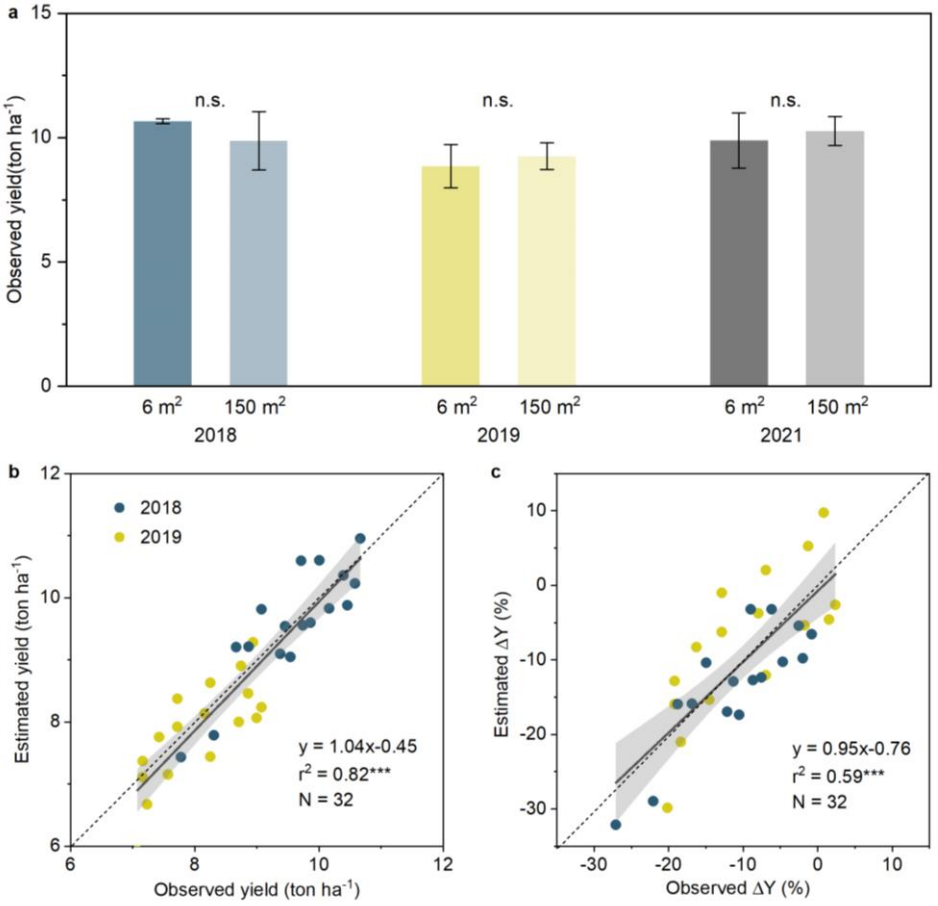

Supplementary Fig. 20 Comparison of yield observations and estimation from yield components. a. Yield observations from adjacent plots owning 6 m^2 and 150 m^2 in 2018, 2019 and 2021 under control. **b**. Observed and estimated yield. **c**. Observed and estimated change in rice yield (ΔY). Column in panel **a** is shown as mean ± standard deviation. The solid line is the best-fit line and shaded area is the 95% confidence interval (estimated from 1,000-time bootstrap analysis), with ***p<0.001. And n.s. for not significant.

References：

1 Lesk, C., Coffel, E. & Horton, R. Net benefits to US soy and maize yields from intensifying hourly rainfall. *Nat Clim Change* **10**, 819-822, doi:10.1038/s41558-020-0830-0 (2020).

2 Li, Y., Guan, K. Y., Schnitkey, G. D., DeLucia, E. & Peng, B. Excessive rainfall leads to maize yield loss of a comparable magnitude to extreme drought in the United States. *Global Change Biol* **25**, 2325-2337, doi:10.1111/gcb.14628 (2019).

3 Beillouin, D., Schauberger, B., Bastos, A., Ciais, P. & Makowski, D. Impact of extreme weather conditions on European crop production in 2018. *Philos T R Soc B* **375**, 20190510, doi:http://doi.org/10.1098/rstb.2019.0510 (2020).

4 Nath, H. K. & Mandal, R. Heterogeneous Climatic Impacts on Agricultural Production: Evidence from Rice Yield in Assam, India. *Asian J Agric Dev* **15**, 23-42, doi:10.22004/ag.econ.275687 (2018).

5 Shi, W. J., Wang, M. L. & Liu, Y. T. Crop yield and production responses to climate disasters in China. *Sci Total Environ* **750**, 141147, doi:10.1016/j.scitotenv.2020.141147 (2021).

6 Troy, T. J., Kipgen, C. & Pal, I. The impact of climate extremes and irrigation on US crop yields. *Environ Res Lett* **10**, 054013, doi:https://doi.org/10.1088/1748-9326/10/5/054013 (2015).

7 Abbas, S. & Mayo, Z. A. Impact of temperature and rainfall on rice production in Punjab, Pakistan. *Environ Dev Sustain* **23**, 1706-1728, doi:10.1007/s10668-020-00647-8 (2021).

8 Davis, K. F., Chhatre, A., Rao, N. D., Singh, D. & DeFries, R. Sensitivity of grain yields to historical climate variability in India. *Environ Res Lett* **14**, 064013, doi:10.1088/1748-9326/ab22db (2019).

9 Tao, F. L. *et al.* Responses of wheat growth and yield to climate change in different climate zones of China, 1981-2009. *Agr Forest Meteorol* **189**, 91-104, doi:10.1016/j.agrformet.2014.01.013 (2014).

10 Tao, F. L., Zhang, Z., Zhang, S. & Rotter, R. P. Heat stress impacts on wheat growth and yield were reduced in the Huang-Huai-Hai Plain of China in the past three decades. *Eur J Agron* **71**, 44-52, doi:https://doi.org/10.1016/j.eja.2015.08.003 (2015).

11 Lobell, D. B., Sibley, A. & Ortiz-Monasterio, J. I. Extreme heat effects on wheat senescence in India. *Nat Clim Change* **2**, 186-189, doi:https://doi.org/10.1038/nclimate1356 (2012).

12 Ji, R. P., Yu, W. Y., Feng, R., Wu, J. W. & Zhang, Y. S. Identification and characteristics of combined agrometeorological disasters caused by low temperature in a rice growing region in Liaoning Province, China. *Sci Rep-Uk* **11**, 9968, doi:10.1038/s41598-021-89227-y (2021).

13 Matiu, M., Ankerst, D. P. & Menzel, A. Interactions between temperature and drought in global and regional crop yield variability during 1961-2014. *Plos One* **12**, e0178339, doi:10.1371/journal.pone.0178339 (2017).

14 Wang, Z. L. *et al.* Drying tendency dominating the global grain production area. *Glob Food Secur-Agr* **16**, 138-149, doi:https://doi.org/10.1016/j.gfs.2018.02.001 (2018).

15 Tian, J. & Huo, Z. G. Index and loss estimation of rain washing damage to early rice pollen in Jiangxi Province. *Journal of Applied Meteorology Science* **29**, 657-666, doi:10.11898/1001-7313.20180602 (2018).

16 Fishman, R. More uneven distributions overturn benefits of higher precipitation for crop yields. *Environ Res Lett* **11**, 024004, doi:10.1088/1748-9326/11/2/024004 (2016).

17 Liu, J. G. *et al.* A high-resolution assessment on global nitrogen flows in cropland. *P Natl Acad Sci USA* **107**, 8035-8040, doi:10.1073/pnas.0913658107 (2010).

18 Fu, J. *et al.* Nationwide estimates of nitrogen and phosphorus losses via runoff from rice paddies using data-constrained model simulations. *J Clean Prod* **279**, 123642, doi:10.1016/j.jclepro.2020.123642 (2021).

19 Bulman, P. & Smith, D. L. Post-Heading Nitrogen Uptake, Retranslocation, and Partitioning in Spring Barley. *Crop Sci* **34**, 977-984, doi:10.2135/cropsci1994.0011183X003400040028x (1994).

20 Salles, C., Poesen, J. & Sempere-Torres, D. Kinetic energy of rain and its functional relationship with intensity. *J Hydrol* **257**, 256-270, doi:10.1016/S0022-1694(01)00555-8 (2002).

21 Lu, D., Yang, Y. J. & Fu, Y. F. Interannual variability of summer monsoon convective and stratiform precipitations in East Asia during 1998-2013. *Int J Climatol* **36**, 3507-3520, doi:10.1002/joc.4572 (2016).

22 Nanko, K., Moskalski, S. M. & Torres, R. Rainfall erosivity-intensity relationships for normal rainfall events and a tropical cyclone on the US southeast coast. *J Hydrol* **534**, 440-450, doi:10.1016/j.jhydrol.2016.01.022 (2016).

23 Sitch, S. *et al.* Recent trends and drivers of regional sources and sinks of carbon dioxide. *Biogeosciences* **12**, 653-679, doi:10.5194/bg-12-653-2015 (2015).

24 GML, *Trends in Atmospheric Carbon Dioxide*, U.S. Department of Commerce (2021), Date accessed: 15th October 2021, https://gml.noaa.gov/ccgg/trends/.

25 Huffman, G. J., Stocker, E. F., Bolvin, D. T., Nelkin, E. J. & Tan, J., *GPM IMERG Final Precipitation L3 Half Hourly 0.1 degree x 0.1 degree V06, Greenbelt, MD*, Goddard Earth Sciences Data and Information Services Center (GES DISC) (2019), Date accessed: 5th August 2021, https://disc.gsfc.nasa.gov/datasets/GPM_3IMERGHH_06/summary.

26 Wang, W. L., *A dataset of ten-day values of crop growth and development and farmland soil moisture in China*, National Meteorological Information Center Meteorological Data Office (2019), Date accessed: 4th November 2019, http://data.cma.cn.

27 Zhan, X. Y. *et al.* Improved Estimates of Ammonia Emissions from Global Croplands. *Environ Sci Technol* **55**, 1329-1338, doi:10.1021/acs.est.0c05149 (2021).

28 Yang, H., Jiang, Z. H. & Li, L. Biases and improvements in three dynamical downscaling climate simulations over China. *Clim Dynam* **47**, 3235-3251, doi:10.1007/s00382-016-3023-9 (2016).

29 Moss, R. H. *et al.* The next generation of scenarios for climate change research and assessment. *Nature* **463**, 747-756, doi:10.1038/nature08823 (2010).

30 FAOSTAT, *Crops and livestock products*, Food and Agriculture Organization of the United Nations (FAO) (2019), Date accessed: 20th September 2019, http://www.fao.org/faostat/en/#home.

31 Vicente-Serrano, S. M., Begueria, S. & Lopez-Moreno, J. I. A Multiscalar Drought Index Sensitive to Global Warming: The Standardized Precipitation Evapotranspiration Index. *J Climate* **23**, 1696-1718, doi:10.1175/2009jcli2909.1 (2010).

32 Wang, S. A. *et al.* Reduced sediment transport in the Yellow River due to anthropogenic changes. *Nat Geosci* **9**, 38-41, doi:10.1038/Ngeo2602 (2016).

33 Jägermeyr, J. *et al.* Climate impacts on global agriculture emerge earlier in new generation of climate and crop models. *Nat Food* **2**, 873-885, doi:10.1038/s43016-021-00400-y (2021).